

1 Precision dynamical mapping using topological data analysis 2 reveals a unique hub-like *transition state* at rest

3
4 Manish Saggar^{a*}, James M. Shine^b, Raphaël Liégeois^c, Nico U. F. Dosenbach^d, Damien Fair^e

5
6 ^aDepartment of Psychiatry and Behavioral Sciences, Stanford University, Stanford, CA, USA

7 ^bBrain and Mind Center, The University of Sydney, Sydney, New South Wales, Australia

8 ^cInstitute of Bioengineering, École Polytechnique Fédérale de Lausanne, Switzerland

9 ^dDepartments of Neurology, Radiology, Pediatrics and Biomedical Engineering, Washington
10 University School of Medicine, St. Louis, MO, USA

11 ^eDepartment of Pediatrics, University of Minnesota Medical School, Minneapolis, MN, USA

12

13

14 * Corresponding Author: saggar@stanford.edu

15

16

17 **Competing Interests Statement:** No conflicts of interest to report.

18

19 **Acknowledgements:** This work was supported by an NIH Director's New Innovator Award
20 (DP2; MH119735), an NIH Career Development Award (K99/R00; MH104605), and an MCHRI
21 Faculty Scholar Award to M.S. The Midnight Scan Club data acquisition was supported by
22 grants from the National Institute of Health (NS088590); the Jacobs Foundation (2016121703);
23 and the Kiwanis Neuroscience Research Foundation to N.U.F.D. Funding for the Human
24 Connectome Project data acquisition were provided by the 16 NIH Institutes and Centers that
25 support the NIH Blueprint for Neuroscience Research (as part of the Human Connectome
26 Project, WU-Minn Consortium; Principal Investigators: David Van Essen and Kamil Ugurbil;
27 1U54MH091657) and by the McDonnell Center for Systems Neuroscience at Washington
28 University. R.L. was supported by the National Centre of Competence in Research - Evolving
29 Language grant (51NF40_180888). D.F. was supported by grants from the National Institute of
30 Health (MH096773, MH115357, and DA041148). The authors thank Timothy O. Laumann,
31 Abraham Z. Snyder, and Ryan V. Raut for discussions and helpful comments on a draft of the
32 manuscript. We also thank Ryan V. Raut for providing processed Midnight Scan Club dataset.

33

34

35 **Tables:** 0

36

37 **Figures:** 7

38

39 **Words** (in the main text): ~6500

40 **Abstract**

41 Even in the absence of external stimuli, neural activity is both highly dynamic and organized
42 across multiple spatiotemporal scales. The continuous evolution of brain activity patterns during
43 rest is believed to help maintain a rich repertoire of possible functional configurations that relate
44 to typical and atypical cognitive phenomena. Whether these transitions or “explorations” follow
45 some underlying arrangement or instead lack a predictable ordered plan remains to be
46 determined. Here, using a *precision dynamics* approach, we aimed at revealing the rules that
47 govern transitions in brain activity at rest at the single participant level. We hypothesized that by
48 revealing and characterizing the overall landscape of whole brain configurations (or states) we
49 could interpret the rules (if any) that govern transitions in brain activity at rest. To generate the
50 landscape of whole-brain configurations we used Topological Data Analysis based Mapper
51 approach. Across all participants, we consistently observed a rich topographic landscape in
52 which the transition of activity from one state to the next involved a central hub-like “transition
53 state.” The hub topography was characterized as a shared attractor-like basin where all canonical
54 resting-state networks were represented equally. The surrounding periphery of the landscape had
55 distinct network configurations. The intermediate transition state and traversal through it via a
56 topographic gradient seemed to provide the underlying structure for the continuous evolution of
57 brain activity patterns at rest. In addition, differences in the landscape architecture were more
58 consistent within than between subjects, providing evidence of idiosyncratic dynamics and
59 potential utility in precision medicine.

60 1. Introduction

61 Spontaneous brain activity in the absence of sensory input is considered to be highly structured
62 in both space and time¹ with amplitudes at least as large as stimulus-driven activity^{2,3}. The
63 ongoing patterns of cortical activity are thought to continually evolve over time and have been
64 shown to encode multidimensional behavioral activity⁴. It is believed that the continuous
65 evolution of cortical activity patterns could reflect multiple functions, namely, recapitulating (or
66 expecting) sensory experiences⁵⁻⁸, maintaining a rich repertoire of possible functional
67 configurations^{9,10}, continuing top-down prediction/expectation signal for updating representation
68 of the world¹, reflecting changes in the behavioral and cognitive states¹¹, and has been shown to
69 be largely bistable¹²⁻¹⁴. However, it is not fully established whether transitions in intrinsic brain
70 activity *follow* some underlying arrangement or instead *lack* a predictable ordered plan.
71 Characterizing the rules underlying transitions in cortical activity has the potential to advance
72 our understanding of the neural basis of cognition, and also to better anchor psychiatric disorders
73 onto more robust biological features^{15,16}.

74
75 Since its inception, functional magnetic resonance imaging (fMRI) has been used to non-
76 invasively measure blood oxygen level-dependent (BOLD) signal as a proxy for neural
77 activity¹⁷. Several fMRI studies have significantly advanced our understanding of brain
78 functioning in healthy and patient populations by successfully identifying static or long-time-
79 averaged measures of intrinsic functional organization¹⁸⁻²³. To measure brain's intrinsic
80 functional architecture, i.e., in the absence of any task (resting-state), co-fluctuations in the
81 BOLD signal are assessed (a.k.a., resting-state functional connectivity). Although the dynamical
82 aspect of brain activity has long been known to be critical in electrophysiology, low
83 spatiotemporal resolution of the human neuroimaging has slowed down embracing dynamical
84 analysis of the brain²⁴. However, time-varying analysis of fMRI data is gathering momentum due
85 to recent advances in data acquisition methods, such as multi-band^{25,26} and multi-echo²⁷ imaging
86 that enhance spatiotemporal resolution of the acquired data and facilitate development of novel
87 data analytics²⁸⁻³⁶.

88
89 Time varying analyses of intrinsic human neuroimaging data have revealed richer dynamics than
90 previously appreciated, including existence of: fast switching between metastable states³⁷;
91 intermittent periods of globally coordinated co-fluctuations across spatially distributed brain
92 regions³⁰; large-scale metastable cortical waves^{24,38}; and hierarchical temporal organization at the
93 group level³⁴. Further, individual differences in time varying signals at rest have been associated
94 with a wide range of cognitive and behavioral traits and even shown to be more sensitive than
95 static (or averaged) functional connectivity²⁹. Typically, a time varying analysis first
96 characterizes a set of brain states at the group level, followed by examining individual
97 differences in frequency or duration of such states. A brain state is typically defined as a
98 transient pattern of whole brain activation (or functional connectivity) and is usually
99 characterized by activation of (or connectivity in) known large-scale brain networks (a.k.a.
100 resting state networks). Importantly, typical time-varying analyses (e.g., using sliding window-
101 based approaches) have been prone to be affected by sampling variability and physiological
102 artifacts in the fMRI data^{39,40}. With that said, however, work using simultaneous wide-field
103 optical imaging and whole-brain fMRI has established a direct link between resting-state
104 hemodynamics in the awake and anesthetized brain and the underlying patterns of excitatory
105 neural activity⁴¹⁻⁴³. Thus, while the ongoing hemodynamics as measured by noninvasive fMRI

106 are coupled to excitatory neural activity, novel methods are required to carefully parse neuronal
107 dynamics while discounting artifactual transitions, with a goal towards deciphering the ‘rules’
108 that determine whole-brain transitions across brain states. For example, it is unclear whether the
109 temporal transitions in brain activity (or connectivity) are best conceptualized as a continuous (or
110 gradual) evolution^{44–46} or discrete (or binary) switches^{47–49}. Further, it is also unclear whether
111 transition from one so-called brain state to another is direct or does the brain pass through a set
112 of intermediary states. Lastly, while previous work defined brain states at the *group level*, it is
113 unclear whether individual differences exist in terms of the configuration of brain states
114 themselves.

115
116 The low spatiotemporal resolution and high complexity of the fMRI data make the study of
117 whole-brain dynamics at the single person level (n=1) a challenging endeavor. Specifically, low
118 signal-to-noise ratio of the BOLD signal⁵⁰ and the typically short duration of resting state fMRI
119 scans (~5-15 min⁵¹) impedes precise characterization at the individual subject level. Further, high
120 cost of MR data acquisition and excessive participant burden limit the amount of data that can be
121 gathered. Fortunately, in the past few years, there is a growing momentum towards collecting
122 and sharing fMRI data using a precision functional mapping approach, where each participant is
123 sampled at multiple occasions (>=10) yielding hours’ worth of data for each individual^{52–55}. Due
124 to the vast heterogeneity in network topology from person to person, these approaches are
125 critical to unveiling basic principles of brain function and organization. We argue that a similar
126 approach for *precision dynamics* will be vital for deciphering the rules regarding how the human
127 brain dynamically adapts from one configuration to the next and how these transitions relate to
128 cognition and various psychopathologies^{56–59}.

129
130 In the current work, using a precision dynamics approach and the Midnight Scan Club (MSC)
131 dataset⁵³, we aimed at revealing the overall landscape of at-rest whole-brain configurations (or
132 states) at the single individual level. We hypothesized that by revealing and characterizing the
133 overall landscape we could interpret the rules that govern transitions in brain activity at rest. The
134 MSC dataset includes individually defined parcellations and ~5 hours of resting state fMRI data
135 for each participant – both of which allowed us to examine the topology and dynamics of at-rest
136 whole-brain configurations in an unprecedented detail. We also addressed previous
137 methodological limitations by using tools from the field of topological data analysis (TDA),
138 which are designed to learn the underlying topology (or shape) of high dimensional datasets that
139 are relatively sparse and noisy^{60,61}. Specifically, here, we used the TDA-based Mapper approach
140 that generates the shape of the underlying dataset as a graph (a.k.a., shape graph)^{32,62,63}. Mapper
141 has been previously shown to capture task-evoked transitions in the whole-brain activity patterns
142 at the highest spatiotemporal resolution³¹. Unlike previous time varying analytics, Mapper does
143 not require splitting or averaging data across space or time (e.g., windows) at the outset. Further,
144 Mapper does not require any a priori knowledge about number of whole-brain configurations and
145 does not impose strict assumptions about mutual exclusivity of brain states³⁷. Lastly, the
146 presented results were not only validated in the MSC dataset using split half analysis, but were
147 also independently validated using a separate dataset from the Human Connectome Project²⁵
148 (n=100, unrelated individuals).

149
150
151

152

153 **2. Results**

154 ***2.1 Estimating reliable landscape of whole-brain configurations at the single participant level***

155 Our first aim was to utilize the TDA-based Mapper approach to reliably estimate individually
156 specific landscape (or manifold) of whole-brain configurations. To ensure the replicability of our
157 findings, we first split the MSC data for each participant into two halves (discovery and
158 replication sets) – each with ~2.5 hours of data per participant. Thus, for each participant, out of
159 a total of ten sessions (each 30 mins long), we assigned odd sessions to the discovery and even
160 sessions to the replication set.

161

162 After rigorous preprocessing (see Methods and Gordon et al.⁵³ for details), the individually
163 specific parcellated data were fed into the TDA-based Mapper pipeline³¹, which consists of four
164 main steps. First, the high-dimensional neuroimaging data are embedded into a lower dimension
165 d , using a non-linear filter function f . Importantly, information loss incurred during
166 dimensionality reduction is putatively recovered during the partial clustering step^{64,65} (third step
167 in the Mapper pipeline). To better capture the intrinsic geometry of the data, a nonlinear filter
168 function based on neighborhood embedding was used³¹ (see Methods for benefits of this non-
169 linear approach). Second, overlapping d -dimensional binning is performed to allow for
170 compression and to reduce any destructive effects of noise. Third, partial clustering within each
171 bin is performed, where the original high dimensional information is used for coalescing (or
172 separating) data points into nodes in the low-dimensional space and hence allows for partially
173 recovering information loss incurred due to dimensionality reduction. Lastly, to generate a
174 graphical representation of the data landscape, nodes from different bins are connected if any
175 data points are shared between them. **Fig. S1** provides step-by-step representation of the Mapper
176 pipeline.

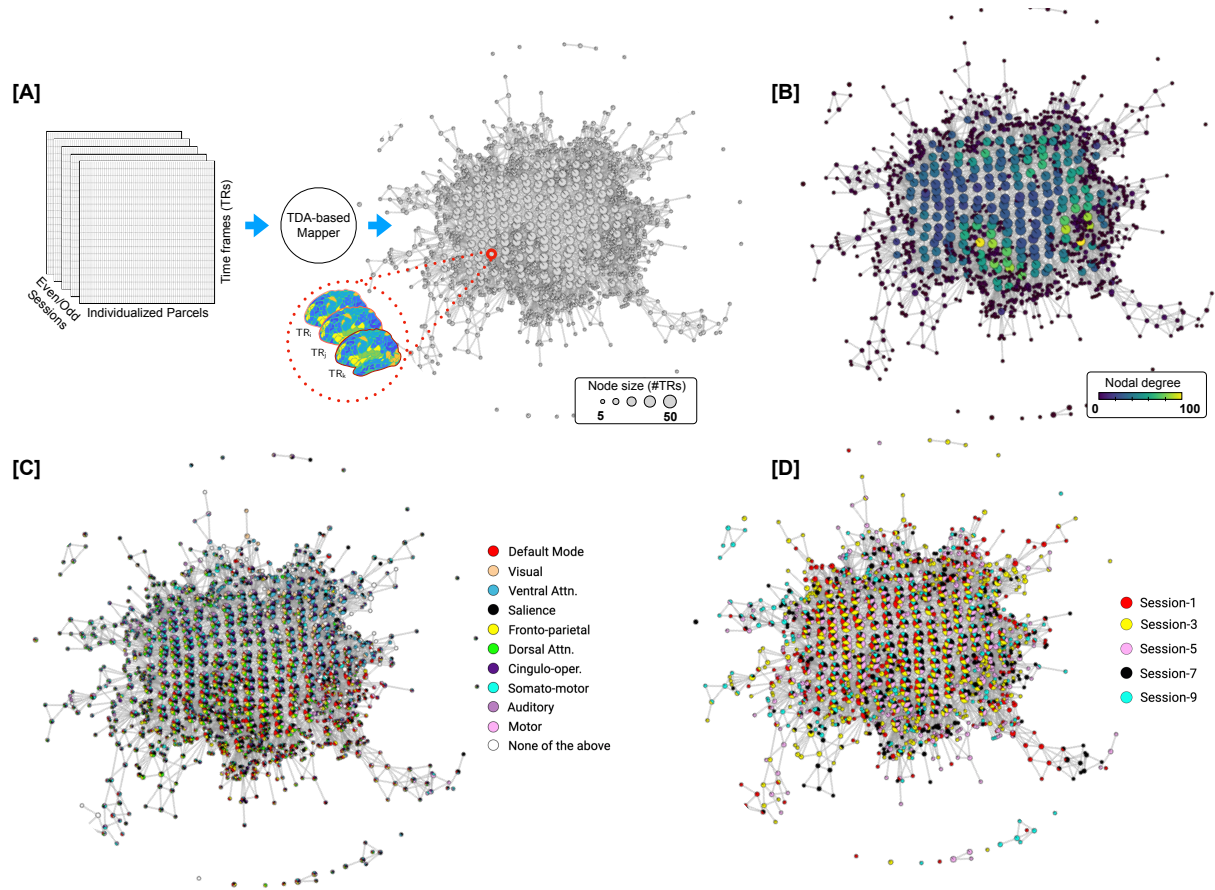
177

178 In contrast to traditional graphical representations of neuroimaging data, nodes in the Mapper-
179 generated shape graph represent clusters of highly similar whole-brain volumes (or time frames
180 (TRs)), and edges connect any two nodes that share one or more whole-brain volumes. This
181 approach naturally embeds temporal patterns within the spatial structure of the graph, which in
182 turn confers several benefits for interrogating the spatiotemporal characteristics of the resting
183 brain. For instance, using this shape graph, we can track how the resting brain dynamically
184 evolves across different functional configurations at the individual-subject level. Importantly, our
185 approach does not require any time-window averaging, which could potentially blur the data and
186 has been shown to lead to artifactual findings due to head movement artifacts and sampling
187 variability^{39,40}.

188

189 To reveal the rules that govern transitions between whole-brain configurations at-rest, we
190 examined: (a) the topological properties of the shape graph, such as the degree distribution and
191 existence of hubs; (b) the relationship between the Mapper embedding and canonical resting
192 state networks; and (c) the transitions between whole-brain configurations. See **Fig. 1** for our
193 analytical approach. In addition to individual variability in the characteristics of Mapper-
194 generated landscapes, we also report the central tendency (or group average) of the dynamical
195 landscape at rest. To account for linear properties of the data (e.g., serial auto-correlation) and
196 sampling variability issues, we compared results with two null models, namely, the phase
197 randomized null⁶⁶ and the multivariate autoregressive null model⁴⁰. Lastly, the results revealed

198 from the MSC dataset were independently validated using a separate dataset from the Human
 199 Connectome Project²⁵ (HCP; n=100 unrelated individuals).
 200



201
 202 **Fig. 1: Estimation and characterization of the dynamical structure underlying transitions in intrinsic**
 203 **brain activity using our TDA-based Mapper approach.** Here, we present data from a representative
 204 participant (MSC-01; odd sessions). [A] Individualized parcellated data from the highly sampled Midnight
 205 Scan Club (MSC) individuals⁵³ was split into two halves: odd sessions (2.5 hours) and even session (2.5
 206 hours) sets. The Mapper approach was independently run on each set to generate the underlying
 207 structure as a graph. Each graph consists of nodes and edges, where the nodes could in turn contain
 208 multiple whole-brain volumes (or TRs; size of a node represents the number of TRs). The nodes are
 209 connected if they share TRs. [B] The Mapper-generated graph can be characterized in several ways. Here,
 210 we examine topological properties by annotating the graph nodes using nodal degree. [C] The graph can
 211 also be annotated with meta-information to characterize the mesoscale structure. Here, we show
 212 annotation using the activation of individual-specific resting state networks (RSNs). A pie-chart based
 213 annotation is used to reveal the proportion of time frames with each node belonging to different RSNs. [D]
 214 Similarly the graph can also be annotated using other available meta-information, e.g., session
 215 information.

216

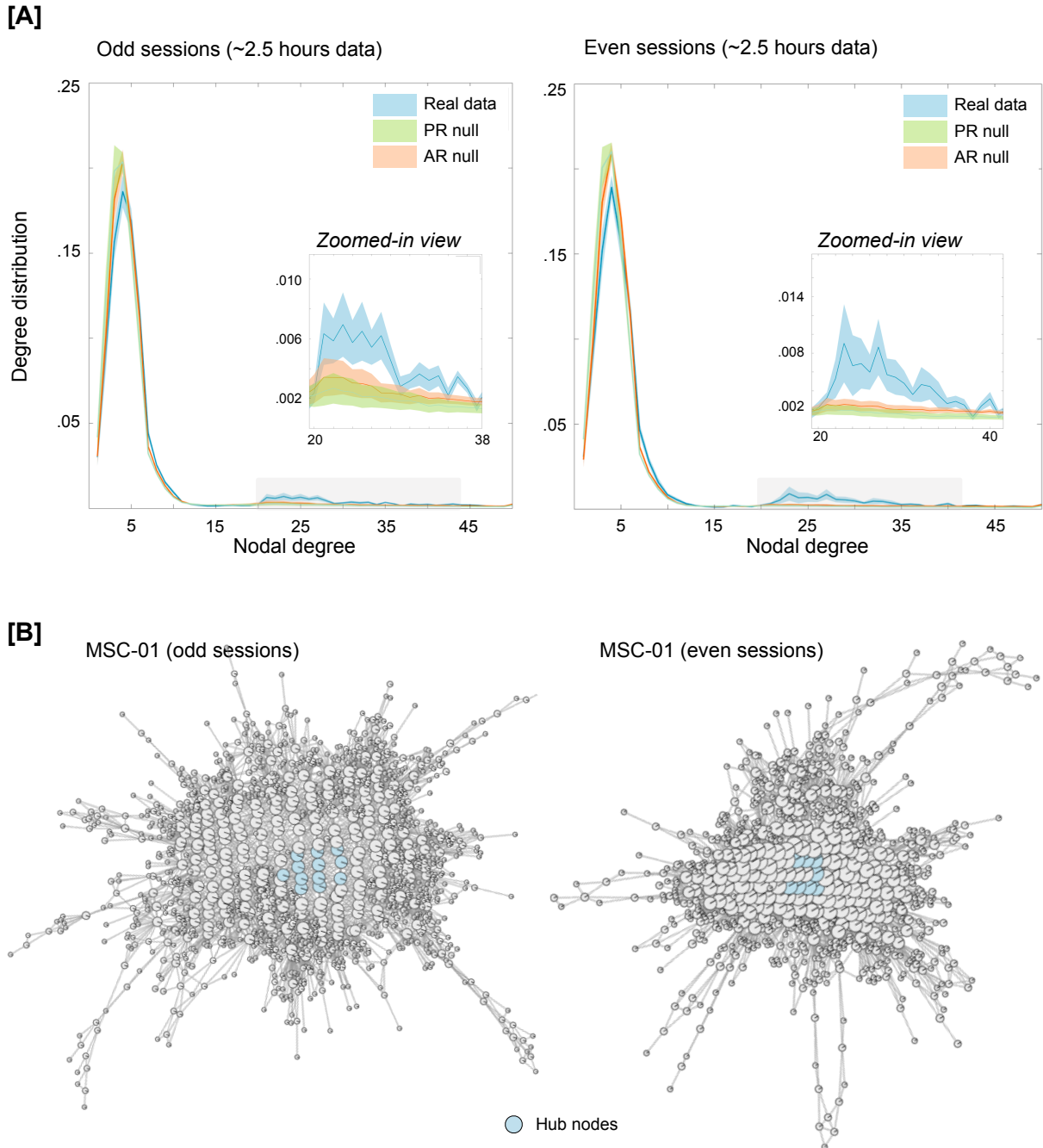
217 **2.2 Topological properties of the landscape reveal existence of hub nodes**

218 We first characterized the Mapper-generated graphs by calculating nodal degree, which measures
 219 the strength (or number) of connections (or edges) per node. In the context of the shape graph,
 220 high degree nodes represent whole-brain activation patterns that are shared by many other nodes
 221 (i.e., are visited often in the temporal evolution of the data). The degree distribution for each
 222 participant and their corresponding splits (odd and even sessions) were further characterized to
 223 determine whether they deviated from what might be expected for linear properties of the data

224 (e.g., autocorrelation in the BOLD signal). We accomplished this goal by comparing the degree
225 distribution from the real data with multiple instances of the two pre-defined null models (phase
226 randomization and multivariate AR model). As evident from the degree distribution plots (**Fig.**
227 **2A**), the real data contained heavy (or fat) tail distributions as compared to both null models. The
228 heavy tail distribution is iconic for most real-world networks and indicates existence of highly
229 connected nodes⁶⁷⁻⁷⁰. This finding was independently replicated in both halves of the MSC data.
230 Statistical difference in the proportion of high-degree nodes (>20) in the real versus null data was
231 assessed using one-way ANOVAs for both odd ($F(2,27)=5.27$, $p=0.012$) and even sessions
232 ($F(2,27)=7.15$, $p=0.003$).

233
234 Highly connected nodes that are also topologically central (i.e., influential) in the graph are
235 known as hub nodes. Hub nodes are hypothesized to act as focal points for the convergence and
236 divergence of information in the network⁷⁰. Existence of hub nodes in the Mapper-generated
237 graph would indicate the presence of nodes (or whole-brain configurations) that are visited often,
238 potentially as intermediate (or transition) state. To examine the existence of hub nodes in the
239 Mapper-generated landscapes, we estimated the closeness centrality of highly connected
240 nodes^{71,72}. This measure associates the nodes with shortest average path lengths as being the
241 most influential (or central) for the graph. Nodes with high closeness centrality can receive
242 information from other parts of the network in a short time (and *vice versa*). Across both halves
243 of the data and all participants, topologically central highly connected hub nodes occurred in the
244 shape graph (**Fig. 2B** highlights the hub nodes in a representative participant and supplementary
245 figure **Fig. S2** shows hub nodes across all MSC participants).

246
247



248
 249 **Fig. 2: Characterizing the Mapper-generated graph using degree distribution.** [A] Degree distributions
 250 averaged across the ten participants, separately for odd and even sessions. For examining linear vs.
 251 nonlinear aspects, two null models were used, namely, the phase randomized null and the multivariate
 252 autoregressive null model. As evident from the degree distribution plots, real data were significantly fat
 253 tailed (>20) compared to both nulls. This finding was independently replicated in both halves of the data.
 254 The shaded area represents standard error around the mean (S.E.M.). [B] Mapper-generated graphs for a
 255 representative participant (MSC-01), highlighting hub nodes (i.e., nodes with high degree (>20) and high
 256 centrality (top 1%). Similar plots were observed across all MSC dataset participants (see Fig. S2).

257
 258 Although substantial data censoring was performed to reduce the impact of head movement
 259 related artifacts, several additional analyses were performed to examine whether the observation

260 of high degree (and hub) nodes was associated with such artifacts. First, we examined whether
261 the presence of high degree nodes was associated with head movement or global signal
262 variations. No difference in framewise displacement (FD) or global signal was observed between
263 brain volumes represented by high and low degree nodes of the shape graph ($ps>0.15$ for FD and
264 $ps>0.75$ for global signal), for either split of the data. Second, we examined whether the
265 percentage of frames censored due to head movement was related with percentage of high degree
266 nodes. No significant relation was observed of either splits of the data ($ps>0.20$). Third, we
267 applied frame censoring to the data generated from null models to examine whether the presence
268 of high degree nodes was merely due to temporal masking. As shown in supplementary **Fig. S5**,
269 high degree nodes were not present in the null data even after frame censoring.

270
271 Further, parameter perturbation analysis was performed to make sure topological properties of
272 the graph were stable across a moderate range of Mapper parameters and the high degree nodes
273 in the real data were not an artifact of Mapper parameters (see Methods). Similar work was
274 previously done to show Mapper-generated graphs were stable across different parameter
275 combinations³¹. As shown in supplementary **Fig. S6**, for a large portion of Mapper parameter
276 values, the proportion of high-degree nodes in the real data were significantly higher than null
277 data.

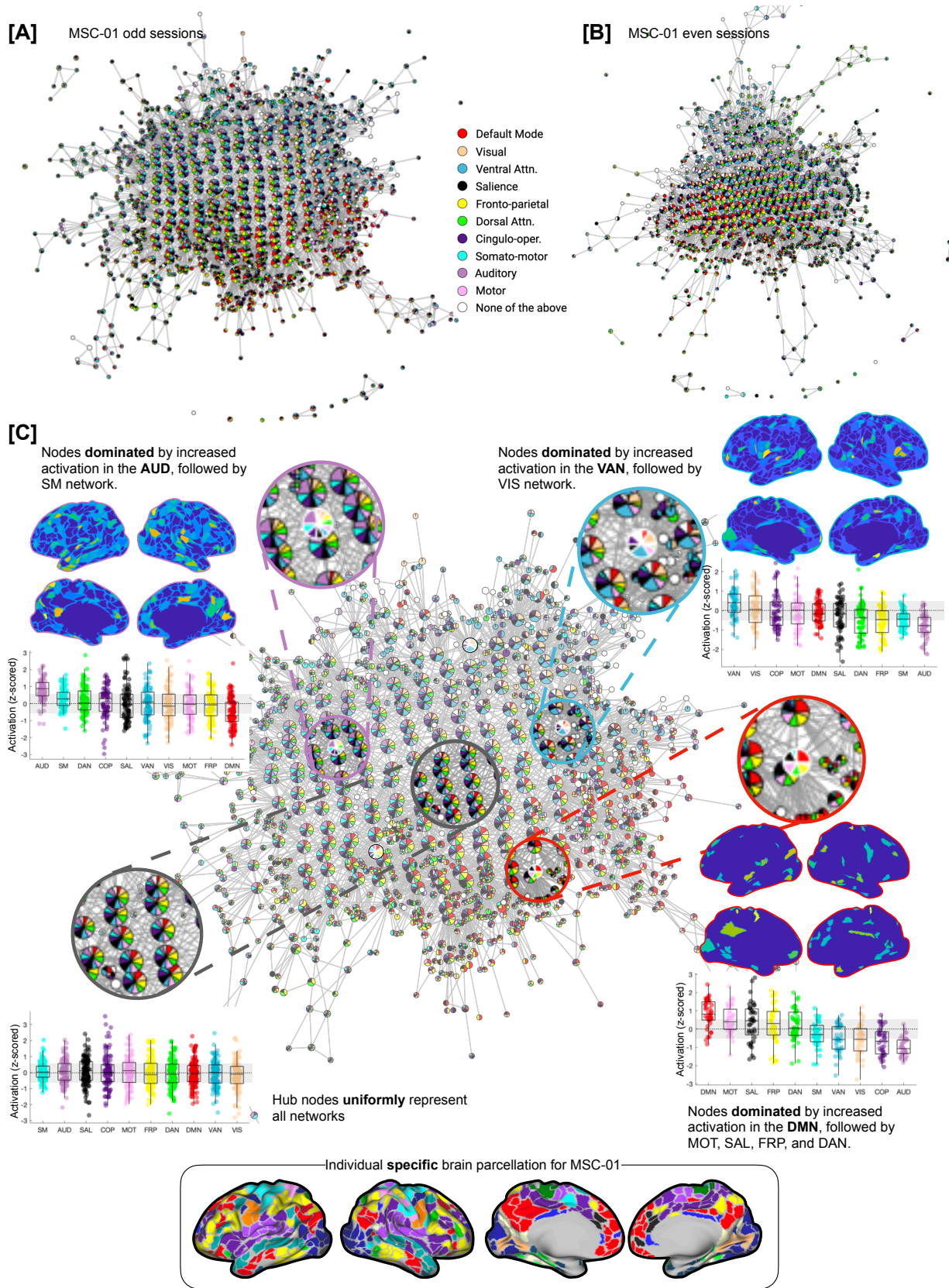
278
279 Overall, the presence of hub nodes in the dynamical landscape (across all participants) provides
280 evidence for whole-brain configurations that i) are often visited during rest; ii) are highly
281 conserved at the individual subject level; and iii) may act as a ‘switch’ between different
282 configurations to putatively organize the spontaneous activity during rest.

283 **2.3 Hub nodes represent uniform (mean) activation across all RSNs, whereas peripheral** 284 **nodes represent increased activation in one (or more) RSNs**

285 To relate Mapper-generated graphs to canonical neuroanatomical depictions of the resting brain,
286 we annotated nodes in the Mapper graph using the relative engagement of a set of canonical
287 large-scale resting state networks (RSNs). Importantly, we leveraged a set of individually-
288 defined network assignments that were pre-defined for individuals in the MSC dataset⁵³. **Fig.**
289 **3A-B** shows a Mapper-generated graph for a representative participant (MSC-01, odd sessions),
290 where each node is annotated by activation in the RSN. In this view, each node is annotated
291 using a pie-chart notation to show the proportion of brain volumes (or TRs) that have any RSN
292 activated (above certain threshold). The mean signal for each RSN was z-scored and a threshold
293 of 0.5 S.D. above the mean was used to denote activation of an RSN (other thresholds produced
294 similar results).

295
296
297 As shown in **Fig. 3C**, the topography of the Mapper-generated landscape provides important
298 insights into the temporal architecture of the resting brain. Topologically highly connected and
299 central hub nodes contained brain volumes in which no characteristic RSN was activated above
300 the mean, whereas nodes with brain volumes dominated by one (or more) RSN(s) tend to occupy
301 the peripheral corners of the landscape. The maps for all individual subjects demonstrated this
302 same basic pattern, although there was evidence to suggest that different combinations of RSNs
303 were dominant in different individuals. For instance, the default mode, ventral attention, and
304 auditory networks clearly dominated the periphery of MSC-01 landscape, across both splits of

305 the data, but other participants had a different combination of networks dominating their
306 landscapes (**Fig. S3**).
307



308
309

310 **Fig. 3: Annotating Mapper-generated graphs based on individual-specific large-scale resting state**
311 **networks (RSNs).** [A-B] Mapper-generated graph for a representative participant (MSC-01; [A] odd and [B]
312 even sessions) are shown. Here, each node is annotated by activation in the known large-scale resting
313 state networks. Each node is annotated using a pie-chart to show the proportion of RSNs activated within
314 each node. As evident, for MSC-01, for both odd and even sessions, the Mapper-generated graph has
315 mainly three networks dominating on the periphery of the dynamical landscape: default mode, ventral
316 attention, and auditory network. [C] Zoomed-in view of the Mapper graph generated using MSC-01 odd
317 sessions. The nodes with dominating RSNs are located more towards the periphery of the landscape,
318 while the hub nodes of the landscape are not dominated by any RSN and rather have uniform mean-level
319 distribution across all RSNs. Four zoomed-in circles highlight four exemplary nodes, where the peripheral
320 nodes have one (or more) RSNs in majority and the central node has no network dominating. Box plots
321 represent activation (z-scored) in the corresponding RSNs across all time frames (TRs) within each
322 highlighted node. We also present *representative* whole-brain activation maps for each of the three
323 peripheral nodes, thresholded using mixture modeling⁷³. The inset on the bottom shows individual-
324 specific parcellation for the participant MSC-01.

325

326

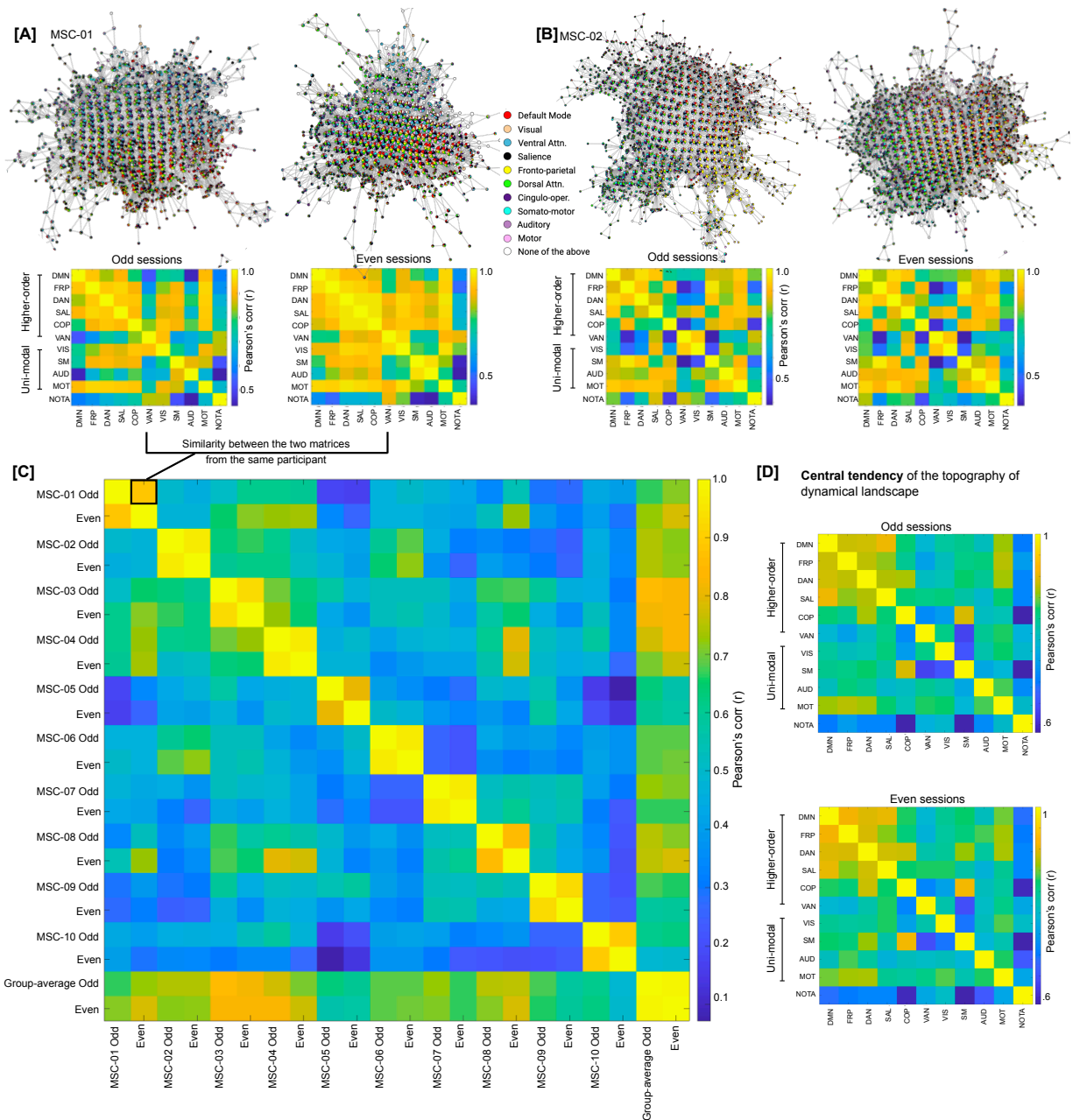
327 **2.4 RSN-based topography of landscapes is highly subject specific and stable across sessions**

328 To quantify the subject-specificity and examine whether Mapper-generated landscapes were
329 stable within participants, we computed similarity between RSNs in terms of their co-
330 localization on the Mapper-generated graphs. If two networks are co-localized on the graph, then
331 they activate (or deactivate) synchronously. **Fig. 4A-B** presents network similarity matrices for
332 three representative participants across their odd and even sessions. As evident, qualitatively, the
333 network similarity matrices are comparable across odd and even sessions. To quantify subject
334 specificity in terms of network similarity, we compared network similarity matrices across
335 sessions and participants using Pearson's correlation. As evident in **Fig. 4C**, high within-
336 participant correspondence (i.e., high similarity between odd and even sessions) for network
337 similarity matrices was observed as compared to between participant correspondence, suggesting
338 dynamical landscapes are subject-specific and stable (over sessions).

339

340 Lastly, we computed the central tendency of the dynamical landscape topography by averaging
341 the network similarity plots across participants. As evident in **Fig. 4D**, the group averaged
342 topography presents a different picture than the individual topographies. Across both halves of
343 the data, group-averaged topography represents more synchrony between higher order cognitive
344 networks (e.g., default mode, fronto-parietal, etc.) than unimodal sensorimotor networks (e.g.,
345 visual, auditory, etc.). However, this discrimination between network types is evident due to
346 group averaging and is not necessarily present at the individual participant level. At the
347 participant level, subject-specific combinations of higher order cognitive networks and unimodal
348 sensorimotor networks are observed to be in synchrony. In summary, individual subjects
349 demonstrated idiosyncratic, yet highly replicable, topological signature at the level of canonical
350 resting state networks.

351

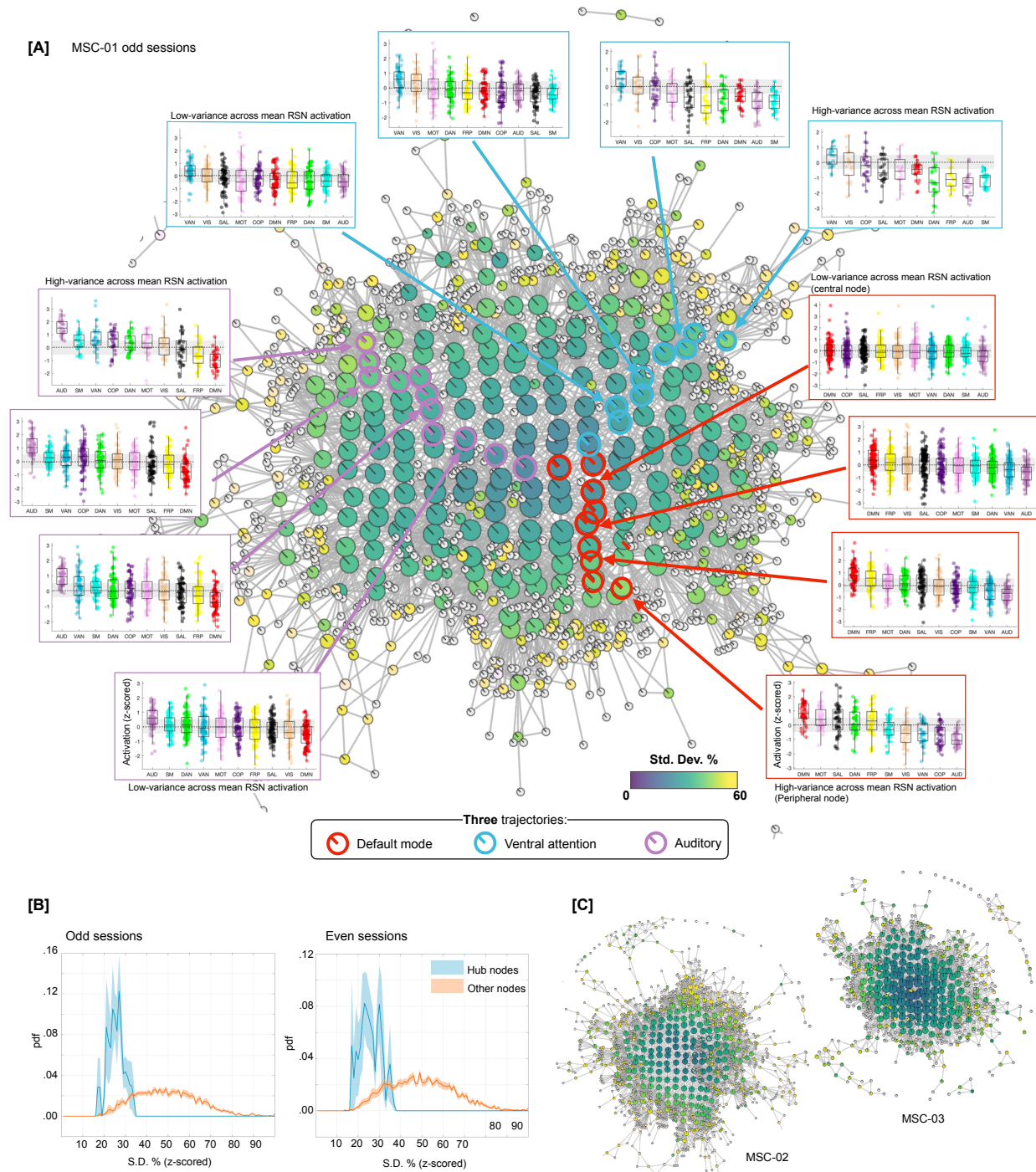


352
 353 **Fig. 4: Dynamical landscapes and their organization are subject specific.** [A-B] Mapper-generated graphs
 354 annotated by RSN activation for two representative participants (MSC01-02) are shown. Both split halves
 355 (odd and even sessions) are shown for each participant. For each half, the figure also shows a similarity
 356 (correlation) matrix between RSNs, where high correlation between two RSNs suggest co-location on the
 357 Mapper-generated graph. As evident through Mapper-graph annotations and between network
 358 correlations there was high degree of similarity between two halves of the same participant. [C] To
 359 quantify between- vs within-participant correspondence across network similarity matrices, network
 360 similarity matrices were compared across split halves from all participants. As shown in the between
 361 subject matrix, high correspondence was observed for within-participant matrices, suggesting dynamical
 362 landscapes demonstrated idiosyncratic, yet highly replicable, topological signature at the level of
 363 canonical resting state networks. [D] Central tendency of the dynamical landscape, averaged over ten
 364 highly sampled individuals, for odd and even sessions.

365
 366

367 **2.5 Traversal on the Mapper-generated landscape revealed a topographic gradient with hub-**
368 **nodes as a putative transition state**

369 Next, we used a variance-based approach to examine whether the traversal on the landscape - i.e.
370 going from one corner to the next (or towards the center) – was smooth (i.e., continuous) or
371 bumpy (i.e., discrete). To this end, we estimated the mean activation for each RSN (across all the
372 brain volumes) within each node, followed by estimating variation (standard deviation; S.D.) in
373 the mean network-level activation across all RSNs. High variance (or S.D.) indicated dominance
374 of one or more RSNs, whereas low variance indicated uniformity across mean RSN activation.
375 As shown in **Fig. 5A** (using a representative participant, MSC-01), annotating Mapper-generated
376 graphs using this variance-based approach revealed a *topographic gradient* in the dynamical
377 landscape, where the peripheral nodes had higher variance with a continual decrease in variance
378 when going towards the center of the graph. To further illustrate the gradient between peripheral
379 dominating nodes and central hub (non-dominating) nodes, using MSC-01, **Fig. 5A** shows three
380 trajectories (one for each of the three dominating networks) and the corresponding boxplots for a
381 sample of nodes from each trajectory – starting from the dominating node on the periphery and
382 moving towards the hub (or non-dominating) nodes. As evident, peripheral nodes represent time
383 frames where one or more RSNs were more activated than others, while as one traverses towards
384 the center of the graph the nodes represent time frames with uniform mean-level activation
385 across all RSNs. **Fig. 5B** shows average distribution of S.D. values, over ten MSC participants,
386 for hub nodes (blue) and other nodes (orange). As evident, the hub nodes had significantly lower
387 S.D. values than non-hub nodes (for both splits of the data; odd: $F(1,18)=132.96$, $p = 9.57 \times 10^{-10}$
388 and even: $F(1,18)=102.7$, $p=7.3 \times 10^{-09}$) – suggesting uniform distribution across all RSNs.
389 Similar gradients were observed across all ten MSC participants (**Fig. 5C** and **Fig. S4**).
390



391
392
393
394
395
396
397
398
399
400
401
402

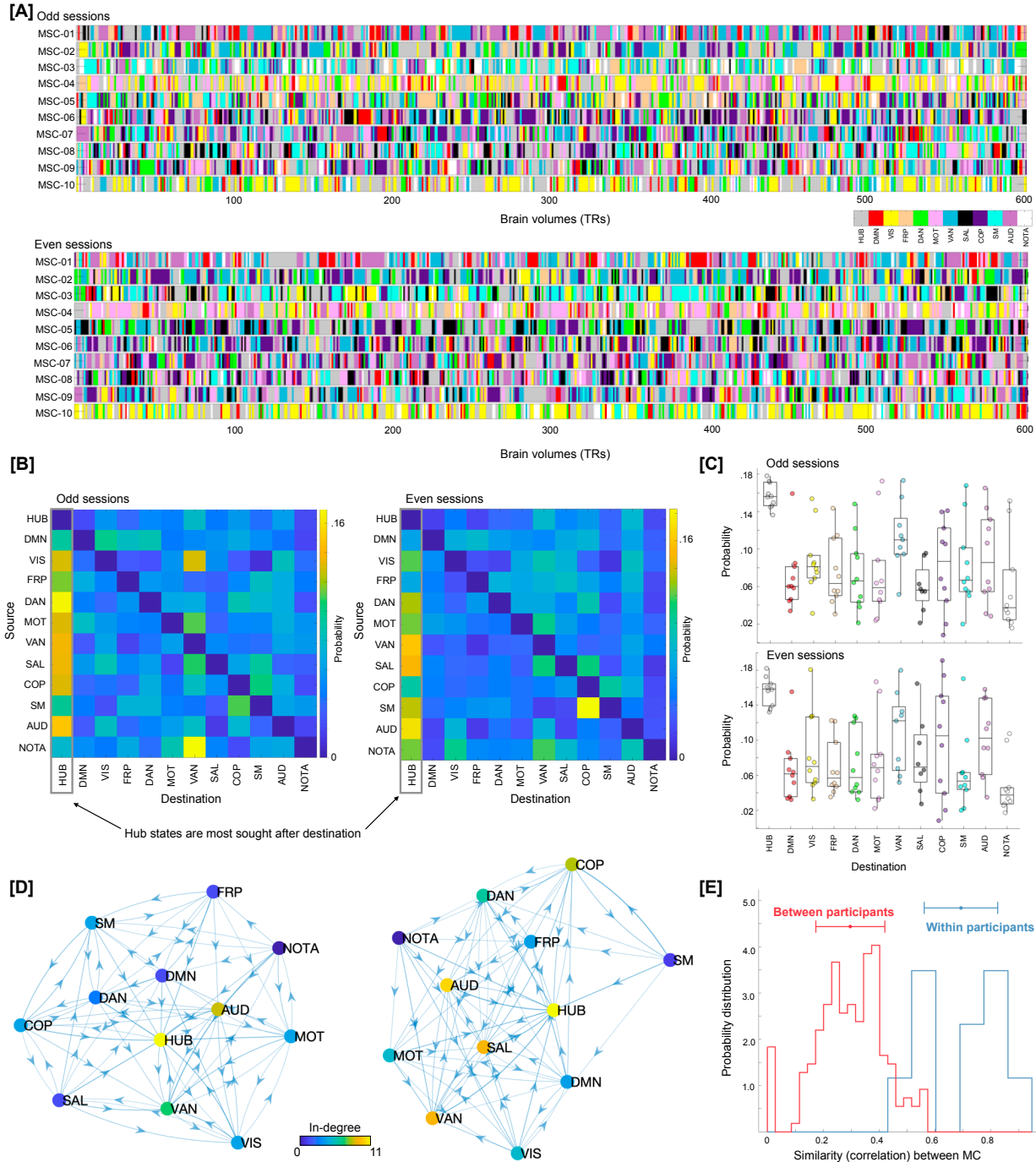
Fig. 5: Annotating the traversal on Mapper-generated landscape using a variance-based approach revealed a dynamical *topographic gradient*. To quantify the variation in RSN-based dominance, we first estimated mean activation for each RSN across the time frames within each node, followed by estimating variation in mean activation across RSNS. High variance (or S.D.) indicated dominance of one or more RSN while low variance (or S.D.) indicated uniformity across RSN activation. **[A]** Annotating Mapper-generated graphs using variance-based approach revealed a dynamical *topographic gradient*, where the peripheral nodes had higher variance with a continual decrease in variance when going towards the center of the graph. The graph is shown from a representative participant (MSC-01; odd sessions). Three trajectories are shown, starting from peak dominance for each of the three RSNS (default mode, ventral attention, and auditory) and ending towards the middle of the graph with nodes of no particular network

403 dominating. Boxplots, for representative nodes on each trajectory, represent activation (z-scored) in the
404 corresponding RSNs across all time frames (TRs) within each represented node. **[B]** Group averaged
405 distribution of S.D. values, over ten MSC participants, for hub nodes (blue) and other nodes (orange) is
406 shown, with S.E.M. as shaded value. Evidently, the hub nodes had significantly low variance across mean
407 RSN activation (indicating uniformly distributed RSN), while the non-hub nodes were highly variant across
408 mean RSN activation. **[C]** Shows variance-based annotation of Mapper graphs for two other participants
409 from MSC dataset (odd sessions). The topographic gradient was observed consistently across
410 participants and for both even and odd sessions (see **Fig. S4**).
411

412 To confirm whether the brain configuration represented by the hub nodes does indeed act as a
413 putative switch, we examined changes in brain activation patterns in the time domain, i.e., at the
414 single time frame (or brain volume) level. The RSN-based proportions from each graph node
415 were propagated to the individual time frames (or TRs) represented by that node. For nodes
416 dominated by any particular RSN, the encompassing TRs were assigned the dominant RSN. For
417 hub nodes, where RSNs were uniformly distributed, the encompassing TRs were assigned a new
418 label (Hub). **Fig. 6A** depicts labels for each TR, across the ten MSC participants, separately for
419 the two splits of the data. To better characterize transitions in RSN-based states we estimated the
420 discrete-time finite-state Markov chains⁷⁴ for each participant and data half. Note the strong
421 visual similarity between rows of the two session matrices.
422

423 **Fig. 6B** shows transition probabilities estimated from the Markov chain estimation averaged
424 across all participants, separately for the two splits of the data. While estimating Markov chains
425 and associated transition probabilities, we ignored putatively artifactual transitions associated
426 with frames discarded due to head movement and due to stitching the sessions together. As
427 evident from the estimated transition probabilities, brain configuration represented by the hub
428 nodes (or our putative transition state) was observed to be the most sought-after destination from
429 any other RSN-dominated state. **Fig. 6C** shows the same result at the individual participant level,
430 such that from any other RSN-dominant state the brain was more likely to transition to the hub
431 transition state – providing evidence for the hub state to be a likely intermediary between any
432 two RSN-dominating states. Transition probabilities can also be represented as a graph (show in
433 **Fig. 6D**). Lastly, we observed the transition probabilities to be highly subject-specific and
434 reliable across sessions (**Fig. 6E**). A one-way ANOVA showed transition probability matrices
435 across the two halves of data were more similar within participant (highly correlated) than across
436 participants ($F(1,398) = 307.86, p=1.83 \times 10^{-51}$).
437

438 In summary, traversal directly on the Mapper-generated landscape revealed a continuous
439 evolution of brain dynamics – a *dynamic topographic gradient*. Similar traversal in the time
440 domain (at single frame level) revealed that the brain configurations represented by hub nodes
441 acted as a putative switch (or a transition state) between different RSN-dominated
442 configurations. Further, the transition probabilities between states were individual-specific,
443 indicating a putative future application in precision medicine.
444
445
446
447
448
449



450
 451 **Fig. 6: Traversal in the temporal domain at the single frame level.** [A] Depicts transitions in brain
 452 activation over time frames in terms of dominant individual-specific RSNs (or hub-like states). Each time
 453 frame (TR) was labeled from the Mapper-generated shape-graphs by propagating the RSN-based
 454 annotation from each graph node to the time frames represented by that node. In addition to RSNs, a new
 455 label representing hub-nodes was also generated. As evident, hub state was often visited by participants
 456 across both data splits. Only showing a subset of timeframes (first 600 frames) for each participant for
 457 ease of viewing. [B] A discrete-time Markov chain was estimated using RSN-based labels for each
 458 participant and data split. While estimating transition probabilities, transitions due to motion censoring
 459 and session boundaries were discarded. Here, we present transition probability matrix averaged over all
 460 10 MSC participants. Diagonals were suppressed to better illustrate transition probabilities across states.
 461 The hub state was observed to be the most sought-after destination from any other state. [C] Boxplots

462 depicting high probability of transitioning into the hub state from any other state, across all participants.
463 **[D]** Estimated Markov chain averaged across all participants. As evident, the hub-state was observed to
464 be most central and with highest in-degree. **[E]** The transition probability matrices (as show in **B**) were
465 reliably estimated at the individual participant level (i.e., high within-participant similarity), indicating a
466 putative application in precision medicine approaches.

467

468 **2.6 Replicating main results in an independent dataset**

469 Although split-half data validation was performed for the MSC dataset, we further replicated the
470 main results in an independent multi-session resting state fMRI dataset (100 unrelated
471 participants from the Human Connectome Project (HCP)²⁵). In the HCP dataset, four 15 min
472 sessions of resting state scans were acquired over a period of two days. Thus, for each individual,
473 we could analyze up to 1 hour of resting state fMRI data. It is important to note that the HCP
474 data were substantially lower in scan duration than the MSC dataset (with 5 hours of resting state
475 fMRI data per individual). Further, instead of using individually-defined parcellation, we used a
476 group parcellation (Gordon atlas with 333 brain regions⁷⁵).

477

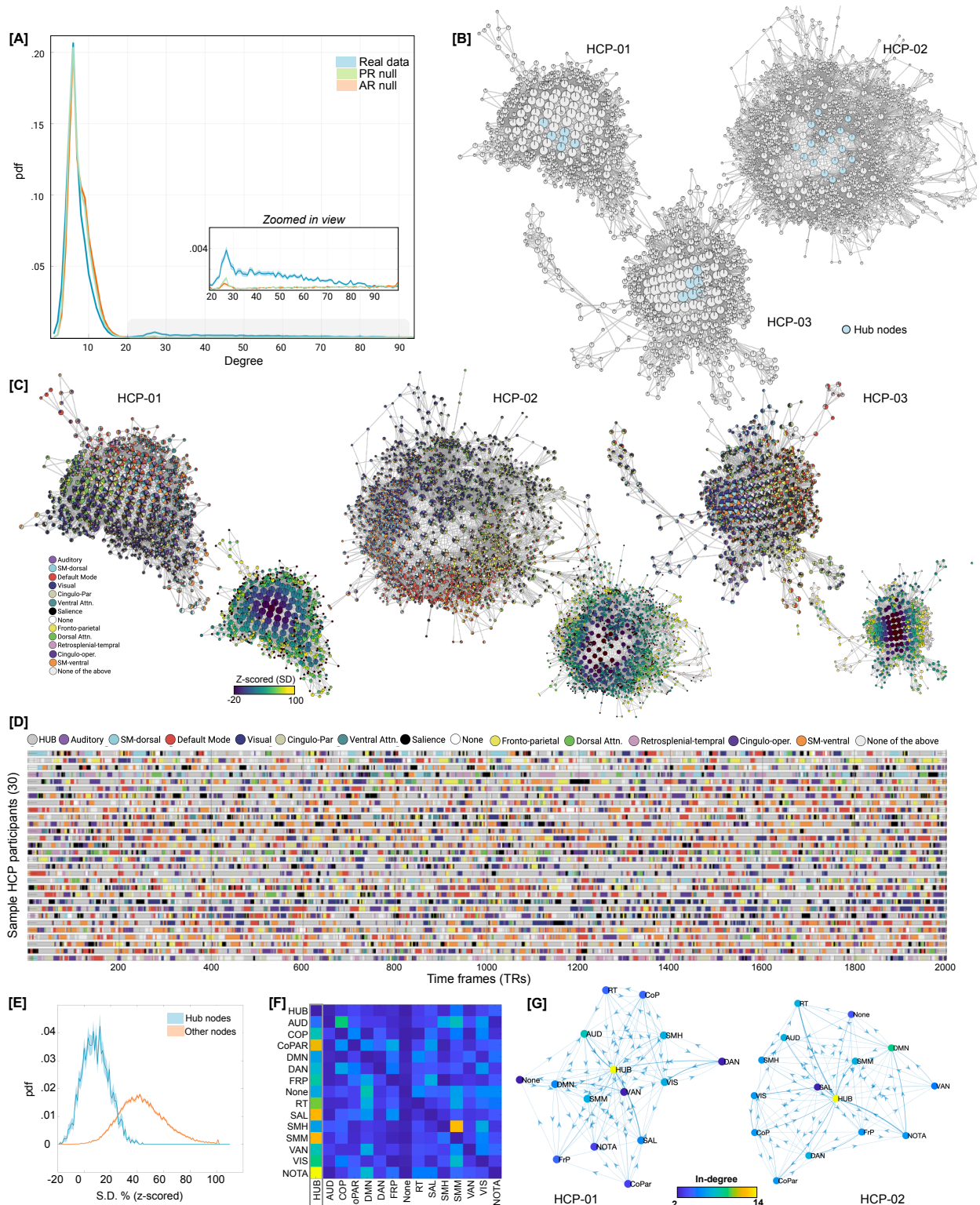
478 After generating Mapper landscapes for each HCP participant, we first compared the degree
479 distribution of graphs generated from real versus null data (from phase randomization and
480 multivariate AR models). Like the MSC data, the HCP data also showed heavy (fat) tail
481 distributions as compared to both null models. Statistical difference in the proportion of high-
482 degree (>20) nodes in the real versus null data was assessed using one-way ANOVA ($F(2, 225)$
483 = 288.11, $p = 8.88 \times 10^{-63}$; **Fig. 7A**). Mapper-generated landscapes from the HCP data also
484 contained hub-nodes (**Fig. 7B**).

485

486 Next, we annotated Mapper-generated graphs using the relative engagement of a set of canonical
487 large-scale resting state networks (RSNs). As opposed to individually-defined networks for the
488 MSC dataset, we used a group parcellation (Gordon atlas with 333 brain regions⁷⁵) for the HCP
489 data. Results are shown for three representative participants in the **Fig. 7C**. We observed highly
490 connected and central hub nodes contained brain volumes where no particular RSN was
491 activated, whereas nodes with brain volumes dominating from one particular RSN tend to
492 occupy the peripheral corners of the landscape. The maps for individual subjects all
493 demonstrated this same basic pattern, although there was evidence to suggest that different
494 combinations of RSNs were dominant in different individuals.

495

496 Lastly, for the HCP dataset, we examined traversal on the landscape as well as temporal
497 evolution of brain activation patterns at the single time-frame level. Using a variance-based
498 approach, as for the MSC-dataset, we again observed a *smooth topographic gradient* in the
499 dynamical landscape of HCP participants, where the peripheral nodes had higher variance with a
500 continual decrease in variance when going towards the center of the graph (**Fig. 7C-D**). For the
501 temporal evolution of brain activation patterns at the single TR level RSN-based proportions
502 from each graph node were propagated to the individual time frames (or TRs) represented by that
503 node. **Fig. 7E** depicts RSN-based labels for each TR, across the 30 representative HCP
504 participants. Using discrete-time finite-state Markov chains, we also estimated transition
505 probabilities, while ignoring putatively artifactual transitions associated with frames discarded
506 due to head movement and due to stitching together sessions. In parallel to the MSC data, the
507 HCP data also provided evidence for the hub-state to be the most sought-after destination from
508 any other RSN-dominated state; thereby providing a putative role of intermediating between
509 other RSN-dominant states (**Fig. 7F-G**).



510
511
512
513
514
515

Fig. 7 Replicating results using an independent dataset from the Human Connectome Project (HCP). [A] Degree distribution of graphs generated from the real versus null data (from phase randomization and multivariate AR models) revealed heavy (fat) tail distributions in the real data. [B] Highlight hub nodes for three representative participants. [C] Annotating Mapper-generated graphs using the relative engagement

516 of a set of canonical large-scale resting state networks (RSNs). Like MSC data, the HCP dataset also
517 revealed that highly connected and central hub nodes contained brain volumes where no particular RSN
518 was activated, whereas nodes with brain volumes dominating from one particular RSN tend to occupy the
519 peripheral corners of the landscape. Using a variance-based approach, like the MSC-dataset, we again
520 observed a *smooth topographic gradient* in the dynamical landscape of HCP participants. **[D]** Traversal in
521 the temporal domain at the single frame level for 30 representative HCP participants. Only showing a sub-
522 set of timeframes for ease of view. Color depicts transitions in brain activation over time frames in terms
523 of dominant individual-specific RSN (or hub-like state). **[E]** Group averaged distribution of S.D. values, over
524 all the HCP participants, for hub nodes (blue) and other nodes (orange) is shown, with S.E.M. as shaded
525 value. **[F]** Group averaged transition probability matrix derived using Markov chains, indicating the hub-
526 state to be the most sought-after destination from any other RSN-dominated state. Diagonal values were
527 set to zero for ease of visualization. **[G]** Estimated Markov chain for two representative participants. As
528 evidence the hub-state was observed to be most central and with highest in-degree.
529

530 **3. Discussion**

531 Understanding how the brain dynamically adapts its distributed activity in the absence of any
532 extrinsic stimuli lies at the core of understanding cognition. Although several innovative
533 approaches have been developed to study the dynamical properties of intrinsic brain activity at
534 rest, the organizational principles governing transitions in spontaneous activity are not fully
535 understood. For example, it is unclear whether transition from one brain state to another is direct,
536 or whether the brain passes through a set of characteristic intermediary states. Further, while
537 previous work defined brain states at the group level, it is unclear whether individual differences
538 exist in terms of how the brain states themselves are configured. Lastly, more work is needed to
539 understand whether temporal transitions in brain activity are best conceptualized as continuous
540 or discrete. To address these foundational questions, using a precision dynamics approach at the
541 single participant level, we constructed the overall landscape of whole-brain configurations at
542 rest. Altogether, four robust findings are observed: (1) across all participants, the landscape of
543 whole-brain configurations contains centrally located hub-nodes that are often visited and likely
544 acted as a *switch* or transition state between different configurations to organize the spontaneous
545 brain activity; (2) transitions occur as a smooth dynamic topographic gradient in the landscape,
546 suggesting a continuous (as opposed to discrete) setup for brain state transitions at rest; (3)
547 importantly transition probabilities between one state to another, at the level of a single time
548 frame, are subject-specific and provide a stable signature of that individual; and (4) while the
549 hub-nodes are characterized by a uniform representation of canonical RSNs, the periphery of the
550 landscape is dominated by a *subject-specific* combination of RSNs (which are also stable across
551 sessions). All the findings reported in this work are corroborated using split-half validation and
552 replication in an independent dataset. Together, using precision dynamics we identify several
553 rules or principles organizing spontaneous brain activity.
554

555 We begin the discussion by first providing a coarse viewpoint of our results that aligns well with
556 previous and more recent works that have identified brain dynamics at rest as a bistable
557 phenomenon. We then dive deeper into the rich subject-specific idiosyncrasies that our work
558 revealed as our approach allowed precision analytics. We then provide a discussion on how our
559 approach can putatively address common limitations of the previous work. Lastly, we provide
560 limitations of our work and avenues for future applications.
561

562 **Coarse viewpoint: bistable brain dynamics at rest**

563 From a coarse vantage point, the presence of low-amplitude (or close to mean activation) hub
564 configurations versus high-amplitude peripheral configurations points towards bistable brain

565 dynamics at rest. This bistable phenomenon is in line with the previous theoretical¹²⁻¹⁴ and recent
566 empirical work that has also shown brain dynamics during the resting state to be predominantly
567 bistable^{34,76,77}. In contrast to the null models, real data revealed significantly higher numbers of
568 hub nodes that were centrally located in the landscape and were representing whole-brain
569 configurations with mean-level activity across all RSNs. The periphery of the landscape, on the
570 other hand, was representative of one or a few dominant RSNs.

571
572 Using Hidden Markov Models (HMM), van der Meer and colleagues recently reported brain
573 dynamics during rest to be primarily driven by whole-brain configurations where all RSNs were
574 uniformly expressed with amplitude close to mean network activities, while configurations with
575 dominant RSNs were only evident sporadically⁷⁶. At the coarse level, our results are in line with
576 these findings as we also observed intrinsic brain activity to be largely driven by whole-brain
577 configurations with uniform RSN representation (i.e., hub-nodes), while configurations with
578 dominant RSNs (i.e., peripheral nodes) were evident sporadically. However, it is important to
579 note that we used precision connectomics data (with longer duration scans) and individual-level
580 definition of brain configurations (as opposed to group-level in case of HMM). These data and
581 methodological enhancements led us to examine finer details about resting brain dynamics as
582 detailed in the next sub-section.

583
584 In another work, also using HMMs, Vidaurre and colleagues found that transitions in intrinsic
585 brain activity are stochastic and cycles between two major meta-states, where the first meta-state
586 was associated with unimodal networks (i.e., sensorimotor) and the second meta-state involves
587 regions related to higher order cognition^{34,78}. Across individuals, the authors observed one of the
588 two meta-states to be dominant, such that the brain cycled between networks within a meta-state
589 more frequently than across meta-states. To anchor the topographical properties of the observed
590 landscape of whole-brain configurations, we computed similarity between RSNs in terms of their
591 co-localization on the Mapper-generated graph. Co-localization of two networks on the Mapper-
592 generated graph implies higher chances of co-activation. As shown in **Fig. 4D**, at the group-
593 level, we also observed a hierarchy of network co-localization, broadly separating unimodal
594 sensorimotor and higher-order cognitive networks. This group-level hierarchy was stable across
595 sessions. However, we also observed individual differences in network co-localization that were
596 highly subject-specific and not exactly following the hierarchy between unimodal and higher-
597 order networks, suggesting the promise of precision dynamics over group-level approaches.

598
599 In another recent work, Esfahlani and colleagues showed bistable brain dynamics at rest using
600 edge-level co-fluctuations. The authors observed the resting brain to oscillate between high- and
601 low-amplitude edge-level co-fluctuations. Further, the authors showed that the relatively short-
602 lived high-amplitude edge co-fluctuations i) drove the functional organization of the resting brain
603 (estimated using functional connectivity; rsFC) ii) were observed to be highly correlated with
604 high-amplitude BOLD (activity) fluctuations; and iii) were more similar within than between
605 subjects^{77,79}. Although we examined transitions in whole-brain activity (as compared to co-
606 fluctuations between regions), we also observed the amplitude-level dichotomy, such that the
607 peripheral nodes of the landscape contained high-amplitude network-specific activations while
608 the hub-nodes contained mean-level low-amplitude activations. We also found that the co-
609 localization of RSNs (primarily driven peripheral nodes) were highly subject specific.

610

611 From the metabolic point of view, Zalesky and colleagues showed that the resting brain
612 dynamically transitions between high- and low-efficiency states³⁰. The high efficiency states
613 were characterized by global coordination across brain regions, thus optimizing information
614 processing at a putatively larger expense of metabolic energy. The low efficiency states on the
615 other hand were characterized by lack of global coordination and putatively requiring minimal
616 metabolic expenditure. Although our results are based on whole-brain activation patterns and do
617 not use sliding windows, the whole-brain configurations represented by hub nodes could
618 putatively require minimal metabolic expenditure due to the low or close to mean activation
619 amplitude, whereas the configurations represented by the peripheral nodes could potentially
620 require high metabolic expenditure as they show high amplitude network-specific activation. It is
621 important to note that the approaches that focus on co-fluctuations between brain regions might
622 miss brain configurations represented by hub-nodes due to their low-amplitude and putatively
623 low co-fluctuations between brain regions. Future work is required to carefully combine
624 activation-based fluctuations in brain dynamics with fluctuations in coordination across brain
625 regions to better understand how changes in network activations relate to co-fluctuations.

626

627 **Fine viewpoint: *rich and idiosyncratic intrinsic brain***

628 Our approach was developed to examine brain activity dynamics at the single participant level,
629 as opposed to previous approaches that have used group-level data to define states^{30,34,76}. Thus,
630 along with precision connectomics data, our precision dynamics approach facilitated finer
631 examination of dynamical organization at rest than before. Although across participants we
632 observed bistable brain dynamics of transitioning between hub and peripheral states, our
633 approach also revealed a large degree of individual variability in terms of the configuration of
634 peripheral nodes. Different combinations of resting state networks dominated peripheral nodes,
635 albeit these combinations were highly subject-specific and consistent across sessions. Further,
636 estimated temporal transition probabilities between RSN-dominated states were also more
637 similar within- than between-participants. Overall, pointing towards future application of our
638 approach in precision medicine.

639

640 Examining the traversal on the landscape as well as across the individual timeframes suggest that
641 the brain configurations represented by hub-nodes were putatively acting as a *transition state*
642 between different parts of the landscape (and respective brain configurations or states). At the
643 single timeframe level, the hub state was also observed to be the most sought-after destination
644 from any other RSN-dominated state. Thus, suggesting a putative intermediary and facilitatory
645 role of the low (or close to mean) amplitude hub states in enabling neural *switching* between
646 high-amplitude RSN-dominated states. Descriptively, the hub-nodes can be thought of serving a
647 role akin to transportation hubs (e.g., the Grand Central Station for trains), such that these hub-
648 nodes facilitate efficient travel as well as cost-effective transportation architecture. It is also
649 possible that the hub nodes represent washout (or recovery) configurations of the brain between
650 high-amplitude brain states represented by the peripheral nodes. Future work using our precision
651 dynamics approach in conjunction with theoretical biophysical modeling⁸⁰ and neuromodulation
652 experiments⁸¹ is needed to better understand how the hub-states facilitate transitions in the
653 intrinsic brain.

654

655 When the Mapper-generated graphs were annotated by variability in mean activation across
656 RSNs, a smooth topographic gradient was consistently observed across all participants. The

657 spontaneous brain activity was observed to be spatiotemporally organized in a continuous
658 gradient with hub- and peripheral-nodes at the opposite ends of the spectrum. Recent work has
659 shown existence of spatial gradients that provide organizational principle for the anatomical
660 organization of large-scale brain networks as a spectrum from unimodal to heteromodal
661 networks⁸². Here, we provide evidence for a dynamical topographic gradient organizing
662 spontaneous brain activity at rest. Looking forward, our precision dynamics approach can be
663 used to understand differences in temporal organization across various mental health disorders.
664

665 **Methodological advances: addressing previous issues**

666 Our TDA-based Mapper approach provides a novel avenue to conceptualize fluctuations in brain
667 dynamics at rest, while addressing several limitations with similarly aimed previous approaches.
668 Broadly speaking, most of the previous approaches conceptualized transitions in the at-rest brain
669 by either estimating inter-regional (or inter-voxel) co-fluctuations over time (e.g., sliding
670 window Pearson's correlation⁴⁴, dynamical conditional correlation⁴⁵, and multiplication of
671 temporal derivatives⁴⁶) or by exploring brain activations on the basis of sparse events (e.g., co-
672 activation patterns⁸³, paradigm-free mapping⁴⁸ and point process analysis⁴⁹). Further, previous
673 work clustered the observed transitions into a set of configurations (or states) at the group level,
674 thereby putatively missing subject-level idiosyncrasies^{30,34,76}. Although several key insights were
675 revealed using previous approaches, e.g., bistability of the resting brain⁷⁶ and applications in
676 clinical realms have been attempted⁸⁴, several methodological limitations were also
677 identified^{28,39,85}. First, it is unclear what spatiotemporal scale is ideally suited for studying brain
678 dynamics, i.e., what window length (or threshold for tagging sparse events) is ideal for
679 measuring transitions²⁸. Further, a priori knowledge is also required to estimate the number of
680 configurations (or states) during clustering. Second, recent work using linearity preserving
681 surrogate data showed that some of the findings recovered using time-varying analysis could be
682 artifactual due to sampling variability^{39,86}. Third, statistical models like HMM also require strict
683 assumptions related to the mutual exclusivity of brain states and require a priori knowledge about
684 number of states⁷⁶.

685
686 Our Mapper-based approach can work directly at the spatiotemporal scale at which the data were
687 acquired and thus bypasses the issues associated with sliding-window based analysis (e.g., how
688 to choose window-length and reduce artifacts related with sampling variability). Recently, a
689 similar Mapper-based approach was shown to capture and track the task-evoked brain dynamics
690 that matched known ground truth transitions associated with the experimental design³¹. Further,
691 our Mapper-based approach also distinguishes itself from the category of exploring dynamics
692 based on sparse events, because the output does not necessarily assume that brain dynamics arise
693 from only a subset of significant events but permits exploration of the *continuous* unfolding of
694 dynamics across each time frame. Further, the Mapper-based approach does not require
695 estimation of correlation (or connectivity) between parcellated brain regions and instead use
696 whole-brain activation maps to extract the overall landscape of brain dynamics. Lastly, no
697 assumptions are required to be made regarding mutual exclusivity of brain states or resting state
698 networks. Instead, Mapper generated graphs can be later annotated (e.g., using pie-chart based
699 visualization) to reveal overlapping communities (or states).

700 **Limitations and future work**

702 Some limitations of our work and associated avenues for future work should also be noted.
703 Although we used a precision individual connectomics dataset to show stable results with ~2.5
704 hours of resting state fMRI data per individual, acquiring that much data from individual patients
705 will initially only be feasible in cases where the clinical needs are very high, e.g., when planning
706 neurosurgical interventions such as resecting epileptic foci. Thus, we also replicated the main
707 findings in an independent cohort from the HCP, with ~1 hour of rsfMRI data per individual.
708 However, future work is required to examine whether our approach would work with datasets
709 that are not as dense (e.g., traditional rsfMRI scans of 10-20 min of rsfMRI data) – potentially
710 leveraging alternative acquisition paradigms⁸⁷.

711
712 Another potential limitation and avenue for future work includes combining activation-based
713 dynamics with co-fluctuation of signal across brain regions. New methods are being developed
714 that can provide fluctuations in functional connectivity at the single frame³⁵. Thus, in the future,
715 TDA-based approaches could be used to combine different degrees of interactions between brain
716 regions ranging from brain activations themselves to higher-order interactions. Future work is
717 also required to better understand what purpose the hub state serves in intrinsic dynamics and
718 whether similar hub states can be seen under other states of consciousness (e.g., anesthesia or
719 sleep). One putative hypothesis could be that the intermittent hub state corresponds to a wash-out
720 period required by the brain before moving from one precise brain configuration to the next.
721 Lastly, due to better signal to noise ratio, we restricted our analysis to cortical activity only.
722 Future work is thus required to include sub-cortical structures and cerebellum to better
723 understand their role in the dynamical organization of the brain.

724
725 Although the topology of Mapper-generated graphs was largely similar across participants, key
726 subject-specific idiosyncrasies were also observed. For example, which networks (or group of
727 networks) dominated the periphery of the landscape was highly subject-specific and reliable
728 across sessions. Further, the Markov chains, estimated from individual time-frame data, were
729 also observed to be not only subject-specific but also reliable across sessions. These results
730 provide preliminary evidence that our Mapper-related approach contains potential utility for
731 precision medicine approaches. Due to the small number of participants in the MSC dataset and
732 only a moderate group size of the HCP cohort used here, we did not attempt to associate
733 topological properties of Mapper-generated landscapes and trait behavior (e.g., intelligence); as
734 large samples are required for reproducible brain-behavioral phenotypic associations⁸⁸. Future
735 work, using data from large consortia (e.g., leveraging the Adolescent Brain Cognitive
736 Development (ABCD) Study; ⁸⁹ (n>11,000)) such brain-behavior associations could be
737 examined.

738 739 **Conclusions**

740 Altogether, we present a novel approach to reveal the rules governing transitions in intrinsic
741 brain activity that could be useful in understanding both typical and atypical cognition. Our work
742 extends previous work both methodologically and conceptually. We observed the dynamical
743 landscape of at-rest brain to contain a shared attractor-like basin that acted like an intermediate
744 state where all canonical resting-state networks were represented equally, while the surrounding
745 periphery had distinct network configurations. Traversal through the landscape suggested
746 continuous evolution of brain activity patterns at rest. Lastly, differences in the landscape

747 architecture were more consistent within than between subjects, providing evidence that this
748 approach contains potential utility for precision medicine approaches.

749

750 References

- 751 1. Ringach, D. L. Spontaneous and driven cortical activity: implications for computation.
752 *Curr. Opin. Neurobiol.* **19**, (2009).
- 753 2. Arieli, A., Shoham, D., Hildesheim, R. & Grinvald, A. Coherent spatiotemporal patterns
754 of ongoing activity revealed by real-time optical imaging coupled with single-unit
755 recording in the cat visual cortex. *J. Neurophysiol.* **73**, (1995).
- 756 3. Chen, Y., Geisler, W. S. & Seidemann, E. Optimal decoding of correlated neural
757 population responses in the primate visual cortex. *Nat. Neurosci.* **9**, (2006).
- 758 4. Stringer, C. *et al.* Spontaneous behaviors drive multidimensional, brainwide activity.
759 *Science (80-.)*. **364**, (2019).
- 760 5. O'Neill, J., Pleydell-Bouverie, B., Dupret, D. & Csicsvari, J. Play it again: reactivation of
761 waking experience and memory. *Trends in Neurosciences* vol. 33 (2010).
- 762 6. Berkes, P., Orbán, G., Lengyel, M. & Fiser, J. Spontaneous cortical activity reveals
763 hallmarks of an optimal internal model of the environment. *Science (80-.)*. **331**, (2011).
- 764 7. Luczak, A., Barthó, P. & Harris, K. D. Spontaneous Events Outline the Realm of Possible
765 Sensory Responses in Neocortical Populations. *Neuron* **62**, (2009).
- 766 8. Han, F., Caporale, N. & Dan, Y. Reverberation of Recent Visual Experience in
767 Spontaneous Cortical Waves. *Neuron* **60**, (2008).
- 768 9. Barttfeld, P. *et al.* Signature of consciousness in the dynamics of resting-state brain
769 activity. *Proc. Natl. Acad. Sci. U. S. A.* **112**, 887–892 (2015).
- 770 10. Hansen, E. C. A., Battaglia, D., Spiegler, A., Deco, G. & Jirsa, V. K. Functional
771 connectivity dynamics: Modeling the switching behavior of the resting state. *Neuroimage*
772 **105**, 525–535 (2015).
- 773 11. Fernandez, L. M. J. *et al.* Highly Dynamic Spatiotemporal Organization of Low-
774 Frequency Activities During Behavioral States in the Mouse Cerebral Cortex. *Cereb.*
775 *Cortex* **27**, (2017).
- 776 12. Freyer, F., Roberts, J. A., Ritter, P. & Breakspear, M. A Canonical Model of Multistability
777 and Scale-Invariance in Biological Systems. *PLoS Comput. Biol.* **8**, (2012).
- 778 13. Freyer, F., Aquino, K., Robinson, P. A., Ritter, P. & Breakspear, M. Bistability and non-
779 Gaussian fluctuations in spontaneous cortical activity. *J. Neurosci.* **29**, (2009).
- 780 14. Valdes, P. A., Jimenez, J. C., Riera, J., Biscay, R. & Ozaki, T. Nonlinear EEG analysis
781 based on a neural mass model. *Biol. Cybern.* **81**, (1999).
- 782 15. Saggat, M. & Uddin, L. Q. Pushing the boundaries of psychiatric neuroimaging to ground
783 diagnosis in biology. *eNeuro* **6**, (2019).
- 784 16. Huys, Q. J. M., Maia, T. V & Frank, M. J. Computational psychiatry as a bridge from
785 neuroscience to clinical applications. *Nat. Neurosci.* **19**, 404–413 (2016).
- 786 17. Chen, J. E. & Glover, G. H. Functional Magnetic Resonance Imaging Methods.
787 *Neuropsychology Review* vol. 25 289–313 (2015).
- 788 18. Filippini, N. *et al.* Distinct patterns of brain activity in young carriers of the APOE-
789 epsilon4 allele. *Proc. Natl. Acad. Sci.* **106**, 7209–7214 (2009).
- 790 19. Yeo, B. T. T. *et al.* The organization of the human cerebral cortex estimated by intrinsic
791 functional connectivity. *J. Neurophysiol.* **106**, 1125–1165 (2011).
- 792 20. Glasser, M. F. *et al.* A multi-modal parcellation of human cerebral cortex. *Nature* **536**,

- 793 171–178 (2016).
- 794 21. Fair, D. A. *et al.* Functional brain networks develop from a ‘local to distributed’
795 organization. *PLoS Comput. Biol.* **5**, e1000381 (2009).
- 796 22. Dosenbach, N. U. F. *et al.* Distinct brain networks for adaptive and stable task control in
797 humans. *Proc. Natl. Acad. Sci.* **104**, 11073–11078 (2007).
- 798 23. Dosenbach, N. U. F., Fair, D. A., Cohen, A. L., Schlaggar, B. L. & Petersen, S. E. A dual-
799 networks architecture of top-down control. *Trends Cogn. Sci.* **12**, 99–105 (2008).
- 800 24. Roberts, J. A. *et al.* Metastable brain waves. *Nat. Commun.* **10**, (2019).
- 801 25. Smith, S. M. *et al.* Resting-state fMRI in the Human Connectome Project. *Neuroimage* **80**,
802 144–168 (2013).
- 803 26. Feinberg, D. A. *et al.* Multiplexed echo planar imaging for sub-second whole brain fMRI
804 and fast diffusion imaging. *PLoS One* **5**, e15710 (2010).
- 805 27. Kundu, P., Inati, S. J., Evans, J. W., Luh, W.-M. & Bandettini, P. A. Differentiating
806 BOLD and non-BOLD signals in fMRI time series using multi-echo EPI. *Neuroimage* **60**,
807 1759–1770 (2012).
- 808 28. Preti, M. G., Bolton, T. A. & Van De Ville, D. The dynamic functional connectome:
809 State-of-the-art and perspectives. *Neuroimage* (2016)
810 doi:10.1016/j.neuroimage.2016.12.061.
- 811 29. Liégeois, R. *et al.* Resting brain dynamics at different timescales capture distinct aspects
812 of human behavior. *Nat. Commun.* **10**, (2019).
- 813 30. Zalesky, A., Fornito, A., Cocchi, L., Gollo, L. L. & Breakspear, M. Time-resolved resting-
814 state brain networks. *Proc. Natl. Acad. Sci.* **111**, 10341–10346 (2014).
- 815 31. Saggat, M. *et al.* Towards a new approach to reveal dynamical organization of the brain
816 using topological data analysis. *Nat. Commun.* **9**, (2018).
- 817 32. Geniesse, C., Sporns, O., Petri, G. & Saggat, M. Generating dynamical neuroimaging
818 spatiotemporal representations (DyNeuSR) using topological data analysis. *Netw.*
819 *Neurosci.* **3**, (2019).
- 820 33. Lurie, D. J. *et al.* Questions and controversies in the study of time-varying functional
821 connectivity in resting fMRI. *Netw. Neurosci.* **4**, (2020).
- 822 34. Vidaurre, D., Smith, S. M. & Woolrich, M. W. Brain network dynamics are hierarchically
823 organized in time. *Proc. Natl. Acad. Sci. U. S. A.* **114**, (2017).
- 824 35. Faskowitz, J., Esfahlani, F. Z., Jo, Y., Sporns, O. & Betzel, R. F. Edge-centric functional
825 network representations of human cerebral cortex reveal overlapping system-level
826 architecture. *Nat. Neurosci.* **23**, (2020).
- 827 36. Casorso, J. *et al.* Dynamic mode decomposition of resting-state and task fMRI.
828 *Neuroimage* **194**, (2019).
- 829 37. Baker, A. P. *et al.* Fast transient networks in spontaneous human brain activity. *Elife* **3**,
830 e01867 (2014).
- 831 38. Muller, L. *et al.* Rotating waves during human sleep spindles organize global patterns of
832 activity that repeat precisely through the night. *Elife* **5**, (2016).
- 833 39. Laumann, T. O. *et al.* On the Stability of BOLD fMRI Correlations. *Cereb. Cortex* (2016)
834 doi:10.1093/cercor/bhw265.
- 835 40. Liégeois, R., Laumann, T. O., Snyder, A. Z., Zhou, J. & Yeo, B. T. T. Interpreting
836 temporal fluctuations in resting-state functional connectivity MRI. *NeuroImage* vol. 163
837 (2017).
- 838 41. Ma, Y. *et al.* Resting-state hemodynamics are spatiotemporally coupled to synchronized

- 839 and symmetric neural activity in excitatory neurons. *Proc. Natl. Acad. Sci. U. S. A.* **113**,
840 (2016).
- 841 42. Lake, E. M. R. *et al.* Simultaneous cortex-wide fluorescence Ca²⁺ imaging and whole-
842 brain fMRI. *Nat. Methods* **17**, (2020).
- 843 43. Kong, X. *et al.* Anatomical and Functional Gradients Shape Dynamic Functional
844 Connectivity in the Human Brain. *bioRxiv* (2021).
- 845 44. Calhoun, V. D., Miller, R., Pearlson, G., Adali, T. & Adalı, T. The chronnectome: time-
846 varying connectivity networks as the next frontier in fMRI data discovery. *Neuron* **84**,
847 262–274 (2014).
- 848 45. Lindquist, M. A., Xu, Y., Nebel, M. B. & Caffo, B. S. Evaluating dynamic bivariate
849 correlations in resting-state fMRI: a comparison study and a new approach. *Neuroimage*
850 **101**, 531–546 (2014).
- 851 46. Shine, J. M. *et al.* Estimation of dynamic functional connectivity using Multiplication of
852 Temporal Derivatives. *Neuroimage* **122**, 399–407 (2015).
- 853 47. Liu, X., Chang, C. & Duyn, J. H. Decomposition of spontaneous brain activity into
854 distinct fMRI co-activation patterns. *Front. Syst. Neurosci.* **7**, 101 (2013).
- 855 48. Petridou, N., Gaudes, C. C., Dryden, I. L., Francis, S. T. & Gowland, P. A. Periods of rest
856 in fMRI contain individual spontaneous events which are related to slowly fluctuating
857 spontaneous activity. *Hum. Brain Mapp.* **34**, 1319–1329 (2013).
- 858 49. Tagliazucchi, E., von Wegner, F., Morzelewski, A., Brodbeck, V. & Laufs, H. Dynamic
859 BOLD functional connectivity in humans and its electrophysiological correlates. *Front.*
860 *Hum. Neurosci.* **6**, 339 (2012).
- 861 50. Parrish, T. B., Gitelman, D. R., LaBar, K. S. & Mesulam, M. M. Impact of signal-to-noise
862 on functional MRI. *Magn. Reson. Med.* **44**, (2000).
- 863 51. Anderson, J. S., Ferguson, M. A., Lopez-Larson, M. & Yurgelun-Todd, D.
864 Reproducibility of single-subject functional connectivity measurements. *Am. J.*
865 *Neuroradiol.* **32**, 548–555 (2011).
- 866 52. Choe, A. S. *et al.* Reproducibility and Temporal Structure in Weekly Resting-State fMRI
867 over a Period of 3.5 Years. *PLoS One* **10**, e0140134 (2015).
- 868 53. Gordon, E. M. *et al.* Precision Functional Mapping of Individual Human Brains. *Neuron*
869 **95**, 791–807.e7 (2017).
- 870 54. Laumann, T. O. *et al.* Functional System and Areal Organization of a Highly Sampled
871 Individual Human Brain. *Neuron* **87**, 657–670 (2015).
- 872 55. O'Connor, D. *et al.* The healthy brain network serial scanning initiative: A resource for
873 evaluating inter-individual differences and their reliabilities across scan conditions and
874 sessions. *GigaScience* vol. 6 (2017).
- 875 56. Damaraju, E. *et al.* Dynamic functional connectivity analysis reveals transient states of
876 dysconnectivity in schizophrenia. *NeuroImage Clin.* **5**, 298–308 (2014).
- 877 57. Demirtas, M. *et al.* Dynamic functional connectivity reveals altered variability in
878 functional connectivity among patients with major depressive disorder. *Hum. Brain Mapp.*
879 **37**, 2918–2930 (2016).
- 880 58. Rashid, B., Damaraju, E., Pearlson, G. D. & Calhoun, V. D. Dynamic connectivity states
881 estimated from resting fMRI Identify differences among Schizophrenia, bipolar disorder,
882 and healthy control subjects. *Front. Hum. Neurosci.* **8**, 897 (2014).
- 883 59. Sourty, M. *et al.* Identifying Dynamic Functional Connectivity Changes in Dementia with
884 Lewy Bodies Based on Product Hidden Markov Models. *Front. Comput. Neurosci.* **10**, 60

- 885 (2016).
886 60. Lum, P. Y. *et al.* Extracting insights from the shape of complex data using topology. *Sci.*
887 *Rep.* **3**, 1236 (2013).
888 61. Carlsson, G. Topology and data. *Bull. Am. Math. Soc.* **46**, 255–308 (2009).
889 62. Singh, G., Mémoli, F. & Carlsson, G. Topological Methods for the Analysis of High
890 Dimensional Data Sets and 3D Object Recognition. *Eurographics Symp. Point-Based*
891 *Graph.* (2007) doi:10.2312/SPBG/SPBG07/091-100.
892 63. Phinyomark, A., Ibanez-Marcelo, E. & Petri, G. Resting-State fMRI Functional
893 Connectivity: Big Data Preprocessing Pipelines and Topological Data Analysis. *IEEE*
894 *Trans. Big Data* **3**, (2017).
895 64. Singh, G., Mémoli, F. & Carlsson, G. E. Topological methods for the analysis of high
896 dimensional data sets and 3d object recognition. *SPBG* (2007).
897 65. Geniesse, C., Sporns, O., Petri, G. & Saggat, M. Generating dynamical neuroimaging
898 spatiotemporal representations (DyNeuSR) using topological data analysis. *Netw.*
899 *Neurosci.* **3**, (2019).
900 66. Prichard, D. & Theiler, J. Generating surrogate data for time series with several
901 simultaneously measured variables. *Phys. Rev. Lett.* **73**, 951–954 (1994).
902 67. Sporns, O. & van den Heuvel, M. P. Network maps of the human brain’s rich club. *Netw.*
903 *Sci.* 1–3 (2013) doi:10.1017/nws.2013.8.
904 68. van den Heuvel, M. P., Bullmore, E. T. & Sporns, O. Comparative Connectomics. *Trends*
905 *Cogn. Sci.* **20**, 345–361 (2016).
906 69. Bassett, D. S. Brain network analysis: a practical tutorial. *Brain* **139**, (2016).
907 70. Fornito, A., Zalesky, A. & Bullmore, E. T. *Fundamentals of Brain Network Analysis.*
908 *Fundamentals of Brain Network Analysis* (2016). doi:10.1016/C2012-0-06036-X.
909 71. Sporns, O., Honey, C. J. & Kötter, R. Identification and classification of hubs in brain
910 networks. *PLoS One* **2**, e1049 (2007).
911 72. van den Heuvel, M. P. & Sporns, O. Network hubs in the human brain. *Trends Cogn. Sci.*
912 **17**, 683–696 (2013).
913 73. Gorgolewski, K. J., Storkey, A. J., Bastin, M. E. & Pernet, C. R. Adaptive thresholding for
914 reliable topological inference in single subject fMRI analysis. *Front. Hum. Neurosci.*
915 (2012) doi:10.3389/fnhum.2012.00245.
916 74. Norris, J. R. Discrete-time Markov chains. in *Markov Chains* (2013).
917 doi:10.1017/cbo9780511810633.003.
918 75. Gordon, E. M. *et al.* Generation and Evaluation of a Cortical Area Parcellation from
919 Resting-State Correlations. *Cereb. Cortex* **26**, (2016).
920 76. Meer, J. N. van der, Breakspear, M., Chang, L. J., Sonkusare, S. & Cocchi, L. Movie
921 viewing elicits rich and reliable brain state dynamics. *Nat. Commun.* **11**, (2020).
922 77. Esfahlani, F. Z. *et al.* High-amplitude co-fluctuations in cortical activity drive functional
923 connectivity. *Proc. Natl. Acad. Sci. U. S. A.* **117**, (2020).
924 78. Majeed, W. *et al.* Spatiotemporal dynamics of low frequency BOLD fluctuations in rats
925 and humans. *Neuroimage* **54**, (2011).
926 79. Betzel, R. F., Cutts, S. A., Greenwell, S. & Sporns, O. Individualized event structure
927 drives individual differences in whole-brain functional connectivity. *bioRxiv* (2021).
928 80. Breakspear, M. Dynamic models of large-scale brain activity. *Nat. Neurosci.* **20**, 340–352
929 (2017).
930 81. Mann, K., Deny, S., Ganguli, S. & Clandinin, T. R. Coupling of activity, metabolism and

- 931 behaviour across the *Drosophila* brain. *Nature* **593**, (2021).
932 82. Margulies, D. S. *et al.* Situating the default-mode network along a principal gradient of
933 macroscale cortical organization. *Proc. Natl. Acad. Sci. U. S. A.* **113**, 12574–12579
934 (2016).
935 83. Liu, X. & Duyn, J. H. Time-varying functional network information extracted from brief
936 instances of spontaneous brain activity. *Proc. Natl. Acad. Sci. U. S. A.* **110**, 4392–4397
937 (2013).
938 84. Du, Y. *et al.* Dynamic functional connectivity impairments in early schizophrenia and
939 clinical high-risk for psychosis. *Neuroimage* (2018)
940 doi:10.1016/j.neuroimage.2017.10.022.
941 85. Keilholz, S. D. Review Article: The Neural Basis of Time-Varying Resting State
942 Functional Connectivity. *Brain Connect.* (2014) doi:10.1089/brain.2014.0250.
943 86. Liégeois, R., Laumann, T. O., Snyder, A. Z., Zhou, J. & Yeo, B. T. T. Interpreting
944 temporal fluctuations in resting-state functional connectivity MRI. *NeuroImage* (2017)
945 doi:10.1016/j.neuroimage.2017.09.012.
946 87. Lynch, C. J. *et al.* Rapid Precision Functional Mapping of Individuals Using Multi-Echo
947 fMRI. *Cell Rep.* **33**, (2020).
948 88. Marek, S. *et al.* Towards Reproducible Brain-Wide Association Studies. *bioRxiv* (2020).
949 89. Casey, B. J. *et al.* The Adolescent Brain Cognitive Development (ABCD) study: Imaging
950 acquisition across 21 sites. *Developmental Cognitive Neuroscience* vol. 32 (2018).
951